



A LETTERS JOURNAL EXPLORING
THE FRONTIERS OF PHYSICS

OFFPRINT

**Far-field fluorescence nanoscopy of diamond
color centers by ground state depletion**

E. RITTWEGER, D. WILDANGER and S. W. HELL

EPL, 86 (2009) 14001

Please visit the new website
www.epljournal.org

TAKE A LOOK AT THE NEW EPL

Europhysics Letters (EPL) has a new online home at
www.epljournal.org



Take a look for the latest journal news and information on:

- reading the latest articles, free!
- receiving free e-mail alerts
- submitting your work to EPL

www.epljournal.org

Far-field fluorescence nanoscopy of diamond color centers by ground state depletion

E. RITTWEGER^(a), D. WILDANGER^(a) and S. W. HELL^(b)

Max Planck Institute for Biophysical Chemistry - Am Fassberg 11, 37077 Göttingen, Germany, EU

received on 14 March 2009; accepted by V. Dose on 17 March 2009
published online 2 April 2009

PACS 42.30.-d – Imaging and optical processing
PACS 07.60.Pb – Conventional optical microscopes
PACS 71.55.-i – Impurity and defect levels

Abstract – We report on two modalities of lens-based fluorescence microscopy with diffraction-unlimited resolution relying on the depletion of the fluorophore ground state. The first version utilizes a beam with a deep intensity minimum, such as a doughnut, for intense excitation followed by mathematical deconvolution, whereas in the second version, a regularly focused beam is added for generating the image directly. In agreement with theory, the subdiffraction resolution scales with the square root of the intensity depleting the ground state. Applied to the imaging of color centers in diamond our measurements evidence a resolving power down to ≈ 7.6 nm, corresponding to 1/70 of the wavelength of light employed. Our study underscores the key role of exploiting (molecular) states for overcoming the diffraction barrier in far-field optical microscopy.

Copyright © EPLA, 2009

Introduction and theory. – Since the work of Abbe [1] it has been widely accepted that the resolution of an optical microscope operating with freely propagating light is limited by diffraction to $\lambda/(2n \sin \alpha) > 200$ nm, with λ denoting the wavelength and $n \sin \alpha$ the numerical aperture of the lens. By abandoning focusing and confining the light-specimen interaction with a tip, near-field optical microscopy [2] enabled subdiffraction imaging of surfaces [3] in a number of applications. However, the non-invasive imaging of the interior of transparent objects remained limited by λ .

The discovery that transitions between elementary molecular states can be effectively used to overcome the limiting role of diffraction [4] has led to the invention of stimulated emission depletion (STED) [5] and ground state depletion (GSD) [6] fluorescence microscopy as tangible concepts for nanoscale imaging with focused visible light. In essence, these concepts separate two or more fluorescently labeled features closer than $\lambda/(2n \sin \alpha)$, by toggling them between a fluorescent “on” and an “off” state [7]. The light beams are prepared such that only the fluorophores of one of these nearby features are “on” during the brief period of time in which their fluorescence is interrogated.

In both concepts, this transient ultrasharp on-off gradient in space is realized with a saturated optical-transition to the off-state. For example, in STED microscopy of organic fluorophores, the on-state is the fluorescent singlet state S_1 whereas the off-state is the singlet ground state S_0 . A “STED beam” of intensity $I(r)$ inducing stimulated emission ($S_1 \rightarrow S_0$) suppresses the prevalence of the S_1 in proportion to $\exp(-I(r)/I_s)$. For intensities $I(r)$ much larger than the characteristic “saturation” intensity I_s , the fluorophores are essentially confined to the ground state and hence not detectable or simply switched off. Preparing the STED beam $I(r)$ with a zero at $r = 0$, *e.g.* as a doughnut with crest intensity I_m and applying $I_m \gg I_s$ confines the emergence of the “on” state to a region of diameter

$$\Delta r \approx \lambda / \left(2n \sin \alpha \sqrt{1 + I_m/I_s} \right) \quad (1)$$

with steep on-off slopes in space, also extending over Δr [7,8]. Scanning the STED beam with a co-aligned beam for excitation across the specimen yields images of subdiffraction resolution Δr . For $I_m/I_s \rightarrow \infty$, it follows $\Delta r \rightarrow 0$, meaning that the limiting role of diffraction is overcome.

The same principle holds for ground state depletion (GSD) microscopy [6,9,10] where the fluorophore is also switched off with a beam featuring a central zero. In the initial proposal [6], switching off is performed by

^(a)Equal contribution.

^(b)E-mail: shell@gwdg.de

transiently shelving the fluorophore in its metastable dark triplet state T_1 . To this end, the excitation from the ground state $S_0 \rightarrow S_1$ is strongly saturated so that the fluorophore is caught in the T_1 via a non-radiative $S_1 \rightarrow T_1$ crossing. Confined to Δr , the ground state fluorophores are read out by a co-aligned excitation beam that is regularly focused to the doughnut center. Scanning the co-aligned beams yields an image with resolution Δr , like in STED microscopy.

In saturated pattern excitation (SPEM) [11] or saturated structured illumination microscopy (SSIM) [12], the ground state S_0 is also depleted by a saturated excitation, but contrary to the previous scheme, the fluorescence generated by this very same transition is recorded. Performed by an array of line-shaped intensity maxima and minima (rather than a doughnut), the saturated excitation at λ yields narrow line-shaped dark regions of dimension Δr which are steeply surrounded by a fluorescence signal giving a “negative” imprint of the features to be imaged. Unlike in STED and GSD microscopy, the final image has to be retrieved mathematically, after turning and scanning the line-array in other directions as well. In SPEM or SSIM, it is the “off” rather than the “on” state that is confined to Δr in space.

Other related concepts utilize the temporal dynamics of the saturated $S_0 \rightarrow S_1$ transition [13] or extract the super-resolution information from the higher harmonics generated by a temporally modulated excitation beam [14]. Switching the fluorophores to the triplet state ($S_0 \rightarrow S_1 \rightarrow T_1$) and recording the position of individually returning molecules to the S_0 enabled a simple far-field fluorescence nanoscopy, called GSDIM [15].

In any case, the essential element of all these concepts is the depletion of the ground state, because the final state elicited by the excitation beam may be multiple or unknown. Moreover, once excited, the fluorophores may be raised to even higher states initiating photobleaching. In fact, photobleaching is the actual challenge of any concept relying on GSD [10,12]. Conversely, as we shall show in this paper, if bleaching reactions are almost absent, GSD offers elegant implementations of far-field optical nanoscopy.

A fluorescent system with negligible photobleaching is presented by NV color centers in diamond [16,17]. Consisting of a charged vacancy next to an impurity nitrogen, and providing optically detectable and orientable spin states, these defects are of great interest because they hold great promise for magnetic imaging [18–20], quantum cryptography [21], and computation [22]. While switching off these centers by STED has enabled their nanoscale imaging [23], here we demonstrate two GSD alternatives implemented with doughnut-shaped focal beams: a single beam “negative” modality requiring mathematical processing and a two-beam counterpart directly providing nanoscale resolution.

Results and discussion. – NV centers in diamond form a molecular-like electronic system with a triplet

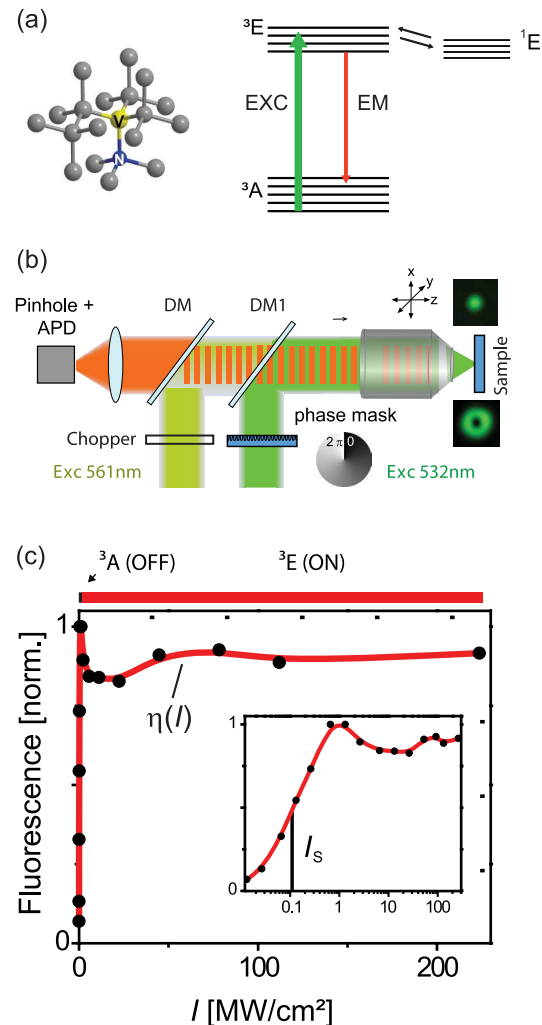


Fig. 1: Ground state depletion of a single nitrogen vacancy (NV) center. a) Energy diagram of a NV center in diamond (inset) with the triplet ground state 3A , the fluorescent state 3E , and the dark singlet state 1E . b) Confocal microscope with red detection and green (532 nm) excitation path merged by a dichroic mirror (DM1). A helical phase ramp converts the focal Airy disk of the excitation beam (upper small panel) into a doughnut (lower panel). While the “negative” GSD modality uses only the doughnut, the direct GSD counterpart uses the Airy disk of a normally focused co-aligned second beam (561 nm) to probe the ground state fluorophores at the doughnut center. Images are obtained by scanning the sample with respect to the beams. c) Excitation (EXC) with intensities I much beyond the saturation intensity I_s (semilogarithmic inset plot) renders a steep onset of fluorescence emission (EM) $\eta(I)$, acting like a switch.

ground state 3A , an excited fluorescent state 3E of $\tau_{fl} = 11.6$ ns lifetime, and a dark singlet state 1E (fig. 1a). The centers can be optically excited at $\lambda = 532$ nm with a cross-section $\sigma \approx 10^{-16}$ cm², which is then followed by fluorescence in the 600–850 nm range [17,24]. With h denoting Planck’s constant and c the vacuum speed of light, the estimated $I_s = hc/(\lambda\sigma\tau_{fl})$ for the $^3A \rightarrow ^3E$ excitation transition is a few hundred kW/cm². This

is easily achieved by focusing a cw beam with a high-aperture lens. For $I < 30I_s$ the centers are known to resist photobleaching [25], but for $I > 30I_s$ photobleaching is still uncharted.

Therefore, we set up a confocal microscope featuring an oil immersion lens of $\alpha = 75^\circ$ (1.46 NA, Leica Microsystems, Wetzlar, Germany), focusing a $\lambda = 532$ nm cw laser beam (Verdi, Coherent Inc., Santa Clara, CA, USA) into a type-IIa diamond grown by chemical vapor deposition. To minimize the background, we replaced the immersion oil with 2,2'-thiodiethanol (TDE) with a 2% water fraction [26]. The fluorescence was collected by the same lens and detected after passing a dichroic filter and a confocal pinhole of 0.3 Airy disks of the emitted light. The diamond was mounted on a 3D-piezo scanning stage with a position accuracy of 0.1 nm and a linearity of 0.03%.

Figure 1c shows the normalized fluorescence $\eta(I)$ of the same NV center for $0 < I < 224$ MW/cm², exceeding the estimated I_s by 1000-fold. As a result, $\eta(I)$ exhibits a steep onset and a plateau due to the depletion of the ³A. $\eta(I) = 0.5$ is obtained for $I_s = 110$ kW/cm² \pm 20%. For $I < 3I_s$, $\eta(I) = 1 - 1/(1 + I/I_s)$ as expected from a saturated transition that is competed by a spontaneous transition in reverse. For $I > 1000I_s$ the NV centers spend only $< 0.1\%$ of their time in the ground state, yet they are photostable. The plateau of $\eta(I)$ is slightly modulated due to intensity-dependent rates to one or more dark states [24], but the decisive factor is that the centers can be steeply switched on by light. Hence, applying an $I(r)$ with a local zero, such as a doughnut or a standing wave, provides a steep gradient between the off- and on-states in space.

To improve the resolution in all directions in the focal plane, we produced a doughnut-shaped $I(r)$ with crest intensity I_m and a central minimum ϵI_m that is ideally zero ($\epsilon < 0.01$) [27]. The minimum was co-aligned with the confocal detection path. Applying $I_m \gg I_s$ increases the absolute values of $I(r)$ throughout the focal region. Wherever $I(r) > 3I_s$, the NV centers are close to the maximum fluorescence, whereas in the region close to the minimum they remain dark. The effective point spread function (PSF) of this imaging modality is given by $h_{\text{eff}}(r, I_m) = h_{\text{det}}(r)\eta(I(r))$, with the detection PSF $h_{\text{det}}(r) \leq 1$ describing the imaging onto the confocal pinhole. For the calculation of Δr under the relevant $I_m > 10I_s$ conditions, the confocality can be ignored and $h_{\text{eff}}(r, I_m) \approx \eta(I(r)) \approx 1 - 1/(1 + I(r)/I_s)$. Moreover, in this case, only the first-order approximation of the minimum matters: $I(r) \approx I_m[\epsilon + (2\beta\pi n/\lambda)^2 r^2]$ [7,8,27]. $0 < \beta < 1$ depends on the aperture angle α and β quantifies the steepness of the minimum; in a flat standing wave $\beta = 1$. Practical β also depends on the perfection of the doughnut implementation. The FWHM of $h_{\text{eff}}(r, I_m)$ is then calculated [28,29] as

$$\Delta r \cong \lambda(\beta\pi n)^{-1} \sqrt{\epsilon + I_s/I_m} \quad (2)$$

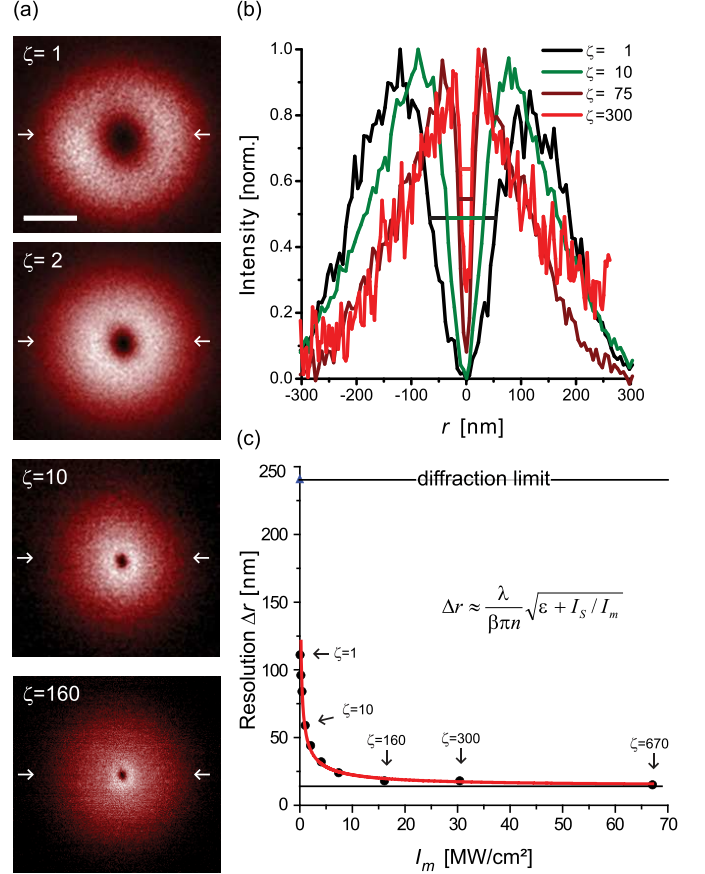


Fig. 2: Effective point spread function (PSF) of the “negative” GSD modality probed by single color centers. a) Increasing $I_m/I_s = \zeta$ renders PSFs with decreasing dark central area Δr ; b) normalized line profiles through the PSFs; c) Δr scales in agreement with eq. (2). The minimum depth $\epsilon = 0.004$ obtained in this experiment allows a resolution of 12 nm $\approx \lambda/44$. Scale bar in a) is 150 nm.

which also quantifies the attainable resolution, as well as the spatial extent over which the centers change their state from “on” to “off”. Δr decreases inversely with $\sqrt{I_m/I_s}$ but reaches its smallest value given by the relative depth of the minimum ϵ . Still, for $\epsilon = 0$ and $I_m/I_s \rightarrow \infty$, it follows $\Delta r \rightarrow 0$.

To test eq. (2) we recorded the images (fig. 2) of single NV centers, *i.e.* $h_{\text{eff}}(r, I_m)$ as a function of $I_m/I_s = \zeta$. The extent Δr of the central region in which the NV centers remain in the ground state scales down with increasing I_m/I_s . The profiles through these effective PSFs also highlight the limiting role of ϵ . The profiles for $I_m/I_s = 160$, 300, and 670 enabled us to extract $\epsilon = 0.004$. Measuring the fluorescence of a single defect excited with an intensity in the linear regime inside the crystal ($n = 2.42$) gave $\beta = 0.35$ for the doughnut minimum. Fitting the measured Δr with eq. (2) exhibits an excellent agreement between the equation and the experiment. The narrowest PSF features $\Delta r = 15$ nm $\approx \lambda/35$.

Next we imaged densely packed NV centers located ≈ 5 microns below the crystal surface using $I_m/I_s = 160$

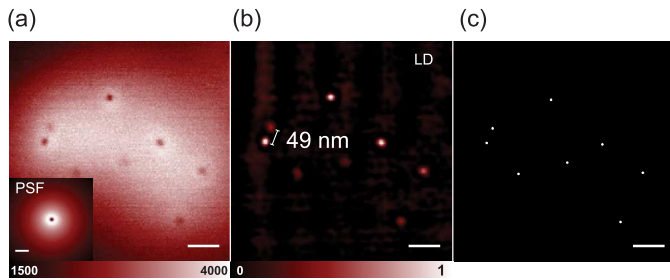


Fig. 3: Inverse GSD nanoscopy of densely packed color centers in diamond. a) Raw “negative” fluorescence image recorded at $I_m/I_s = 160$, exhibiting the centers as dips. Linear deconvolution with the calculated PSF (inset) renders a positive image (b). Note that correct mapping of the position and brightness of the centers requires the deconvolution. Given that (b) represents individual centers, calculation of their centroid refines their coordinate, here to ≈ 1 nm precision. Scale bar is 150 nm.

(fig. 3a). As anticipated, the defects are witnessed as nano-sized dark spots in an extended bright area. Mandatory deconvolution with $h_{\text{eff}}(r, I_m)$ renders the actual image (fig. 3b). Given that all imaged centers are separated and that the recording is not compromised by scanning distortions, the coordinates of each center can be refined by computing the centroid of each spot [23,30,31], here to a precision of ≈ 1 nm.

Our second GSD version renders the image directly. To this end, we employ a regularly focused second excitation beam probing the fluorophores that, being located at the doughnut minimum, have remained in the ground state. We opted for $\lambda = 561$ nm (instead of 532 nm) because this wavelength is conveniently coupled into the excitation path by a second dichroic mirror and is closer to the excitation maximum of the NV centers. Modulating this beam at 1 kHz and recording the elicited fluorescence with a lock-in amplifier (10 ms time constant) extracted the signal from the Δr -sized region at the doughnut minimum. The effective PSF is $h_{\text{eff}}(r, I_m) = h_{\text{det}}(r)[1 - \eta(I(r))]$, with a FWHM Δr given by eq. (2). Imaging individual NV centers (fig. 4) revealed the experimental $h_{\text{eff}}(r, I_m)$. Fitting eq. (2) with $\beta = 0.35$ and $\epsilon \approx 0$ to the measured Δr validated again the increase in resolution in proportion to $\sqrt{I_m/I_s}$.

Figure 5 compares a confocal recording with its GSD counterpart delivering direct images at $\Delta r = 14$ nm resolution in the focal plane. The GSD image is the sum of three subsequent recordings with a pixel dwell time of 25 ms. The 15-fold increase in resolution over that of confocal ($\Delta r = 212$ nm) microscopy directly discerns individual NV centers located only 27 nm apart (fig. 5b). While no explicit data processing is required in this case, applying an optional nonlinear Richardson-Lucy deconvolution [32] further improves the image (fig. 5c).

The limits set by ϵ can be lessened by replacing the cw beam with a pulsed beam featuring pulses that are somewhat shorter than about one-third of the lifetime of the targeted excited state. In this case fluorescence

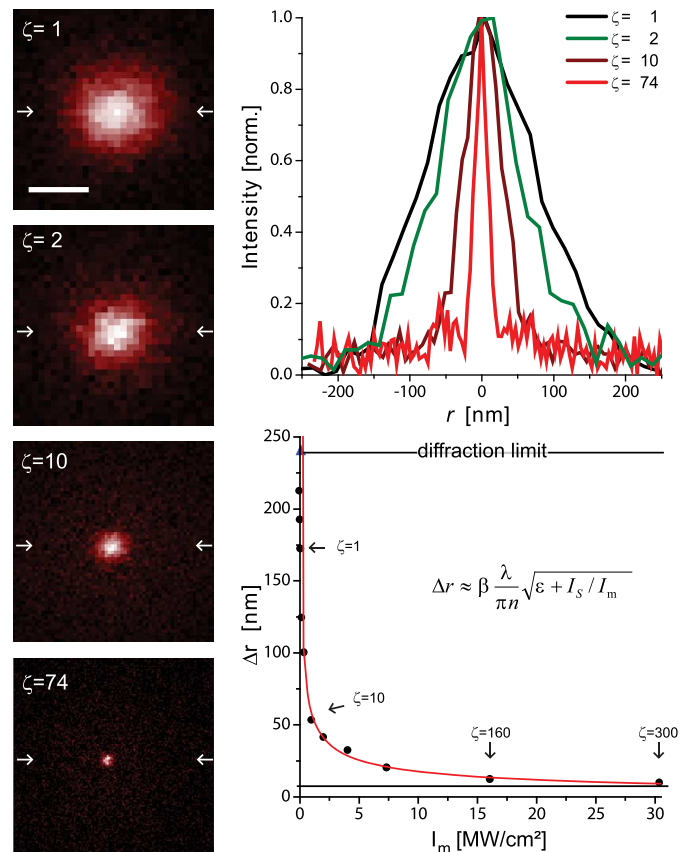


Fig. 4: Effective PSF and resolving power of direct GSD microscopy probed by single color centers. a) Increasing $I_m/I_s = \zeta$ renders PSFs with decreasing FWHM Δr ; scale bar equals 150 nm. b) PSF line profiles. c) Δr scales inversely with $\sqrt{I_m/I_s}$ approaching 9.5 nm.

on-switching by GSD follows $\exp(-I/I_s)$, as in ideal STED [23]. Pulsed illumination also affords higher I_m at moderate average power.

ϵ can also be minimized by removing aberrations, as was exerted for recording the direct GSD image (fig. 6) of a single NV center at $I_m/I_s = 910$. Representing an effective PSF of $\Delta r = 7.6$ nm, the image proves the ability of direct GSD to image with single-digit nanometer resolution.

Whereas in the negative modality the image is derived from the fluorophores outside Δr , in direct GSD and STED microscopy the image signal stems from the probed area Δr around the doughnut zero. This is an important advantage because the fluorescence carries information from the probed area; in the case of the NV centers the fluorescence intensity indicates the spin state.

Due to the way it is produced, the doughnut actually assumes a tubular shape extending in the z -direction [27]. Consequently, increasing I_m also imparts larger intensities in the z -direction. In the negative imaging case, defects located above and below the focal plane are then increasingly captured by the doughnut, meaning that the axial resolution deteriorates. Moreover, since the I_m in a particular xy -plane decreases with increasing z , Δr

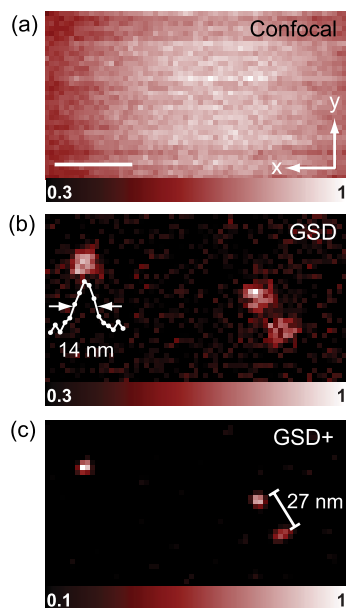


Fig. 5: Direct GSD nanoscopy of diamond color centers. While the a) confocal image ($\Delta r \approx 212$ nm) is featureless, the 14 nm spatial resolution of the corresponding direct GSD image shown in b) reveals three color centers. Two of them are 27 nm apart and clearly resolved by direct GSD nanoscopy. c) Positivity-constrained deconvolution improves the image contrast. Scale bar equals 50 nm.

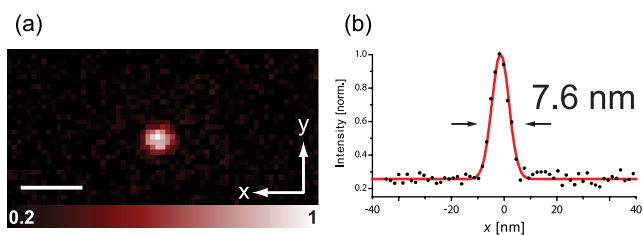


Fig. 6: Effective PSF in direct GSD nanoscopy with $\epsilon \approx 0$. a) Image of a single NV center obtained by summing 7 consecutive recordings of the same area; b) line profile along the x -axis proves resolution potential of $\Delta r = 7.6$ nm as an upper limit. Scale bar is 20 nm.

increases accordingly. Given that the features are single centers, their z -position can be derived from the defocus, especially if the doughnut bears a z -dependent aberration such as astigmatism. In contrast, featuring a confocal detection path, the direct GSD modality discriminates the focal plane with depth $\approx \lambda$, thus providing 3D imaging like a confocalized STED setup. However, unlike the latter, the direct GSD modality can be operated with a single wavelength because it employs just excitation, *i.e.* on-switching. Unfortunately, this convenience also poses challenges because weakly fluorescent objects are difficult to discern from bright neighbors with inherently large absolute noise levels. STED microscopy has an advantage in this regard, because decreasing the on-state area by off-switching affords measurement against low background.

Utilizing saturated transitions or switching, GSD and STED microscopy are readily tagged as nonlinear optical methods. However, this categorization is imprecise, because these concepts radically diverge from multiphoton absorption or scattering microscopy which relies on the joint action of $m > 1$ photons and, as a matter of fact, has failed to provide resolution on the nanoscale [33]. In STED and GSD microscopy, the key element is different: fluorophores that are closer than the diffraction limit are optically prepared such that, at the time point of detection, they can be distinguished by their states: ($S_0 \rightarrow S_1$); ($S_0 \rightarrow T_1$); (${}^3A \rightarrow {}^3E$); (*cis* \rightarrow *trans*), etc. Hence, the role of the optically induced switch is to deliver for a brief period of time a steep gradient of disparate states in space [7,33]. The optical switching transition can be implemented in both directions, which becomes obvious when comparing STED with GSD. Since the states employed for separation are on-off pairs, the adjacent fluorophores inevitably must be registered sequentially in time. In STED and GSD microscopy this is accomplished by scanning the “on” or “off” state region of extent Δr (or the on-off gradient extending over Δr) across the object in space.

Thus, STED and GSD microscopy radically differ from near-field optical microscopy because unlike the latter, they operate with Δr -sized gradients or spots of states, rather than with Δr -sized gradients or spots of light. Preparing adjacent fluorophores in different states by on-off switching of single molecules is also the cornerstone of the more recent single molecule switching concepts [33–35]. Whereas the latter switch the molecule stochastically in space, in STED and GSD the switching occurs at a coordinate defined by the local minimum of the beam that is responsible for the optical switching. Clearly, STED and GSD microscopy have far more in common with the single molecule switching nanoscopy modalities than with multiphoton microscopy.

The central role of the states also explains why the attainable resolution depends so much on the fluorophore itself [4–7,28]. The nanometric imaging of NV centers reported herein, and possibly of other color centers in the future, is largely due to their excited-state photostability. Importantly, these centers offer many more states and transitions to be exploited, such as metastable electronic dark states [7,28] entailing lower intensity values I_s . This strategy has proved workable for organic fluorophores in the initial GSD concept [6,10] and has also been extended to switching photochromic compounds and fluorescent proteins [7,28]. Likewise, one could use dark states to switch the NV centers stochastically, as in the concept GSDIM [15]. The photostability and paramagnetism of their basic states shall also enable the use of other transitions in NV centers that are too weak in organic fluorophores or simply compromised by photobleaching. For example, the application of a static magnetic or electric field gradient —as opposed to an optical field gradient β — is expected to encode the spatial position in

a Zeeman- or Stark-shift [19,36] like in nuclear magnetic imaging [37]. Conversely, the fluorescence of NV centers can be used to sense local magnetic fields [18–20], while direct GSD imaging could possibly be used to read them out.

Although GSD or STED microscopy have initially been designed for fluorescence imaging, fluorescence is not an essential element of these concepts. The requirements are that the material to be imaged can be optically transferred between two states [5,6,28] and that at least one of these states can be detected through a characteristic signal. This signal need not be fluorescence, in fact, not even optical, because the decisive point is the defined transfer between the states. Clearly, the specifics of the NV centers have been key to demonstrating nanometer resolution by these ground state depletion concepts. Therefore, this study proves once more the importance of selecting the suitable states and transitions [4–7,33] for realizing diffraction-unlimited resolution with focused visible light.

We thank V. WESTPHAL for designing a part of the electronic equipment, J. KELLER, C. EGGELING and K. Y. HAN for valuable discussions. A SCHÖNLE is thanked for the ImSpector software and F. JELEZKO (University of Stuttgart) for providing the crystal. DW acknowledges a doctoral fellowship by the German National Academic Foundation.

REFERENCES

- [1] ABBE E., *Arch. Mikrosk. Anat.*, **9** (1873) 413.
- [2] SYNGE E. H., *Philos. Mag.*, **6** (1928) 356.
- [3] POHL D. W., DENK W. and LANZ M., *Appl. Phys. Lett.*, **44** (1984) 651.
- [4] HELL S. W., *Opt. Commun.*, **106** (1994) 19.
- [5] HELL S. W. and WICHMANN J., *Opt. Lett.*, **19** (1994) 780.
- [6] HELL S. W. and KROUG M., *Appl. Phys. B*, **60** (1995) 495.
- [7] HELL S. W., *Nat. Biotechnol.*, **21** (2003) 1347.
- [8] WESTPHAL V. and HELL S. W., *Phys. Rev. Lett.*, **94** (2005) 143903.
- [9] HELL S. W., *Increasing the resolution of far-field fluorescence light microscopy by point-spread-function engineering*, in *Topics in Fluorescence Spectroscopy*, edited by LAKOWICZ J., Vol. **5** (Plenum Press, New York) 1997, pp. 361–422.
- [10] BRETSCHNEIDER S., EGGELING C. and HELL S. W., *Phys. Rev. Lett.*, **98** (2007) 218103.
- [11] HEINTZMANN R., JOVIN T. M. and CREMER C., *J. Opt. Soc. Am. A*, **19** (2002) 1599.
- [12] GUSTAFSSON M. G. L., *Proc. Natl. Acad. Sci. U.S.A.*, **102** (2005) 13081.
- [13] ENDERLEIN J., *Appl. Phys. Lett.*, **87** (2005) 094105.
- [14] FUJITA K., KOBAYASHI M., KAWANO S., YAMANAKA M. and KAWATA S., *Phys. Rev. Lett.*, **99** (2007) 228105.
- [15] FÖLLING J., BOSSI M., BOCK H., MEDDA R., WURM C. A., HEIN B., JAKOBS S., EGGELING C. and HELL S. W., *Nat. Methods*, **5** (2008) 943.
- [16] GRUBER A., DRBENSTEDT A., TIETZ C., FLEURY L., WRACHTRUP J. and VON BORCZYKOWSKI C., *Science*, **276** (1997) 2012.
- [17] JELEZKO F. and WRACHTRUP J., *Phys. Status Solidi A*, **203** (2006) 3207.
- [18] TAYLOR J. M., CAPPELLARO P., CHILDRESS L., JIANG L., BUDKER D., HEMMER P. R., YACOBY A., WALSWORTH R. L. and LUKIN M. D., *Nat. Phys.*, **4** (2008) 810.
- [19] BALASUBRAMANIAN G., CHAN I. Y., KOLESOV R., AL-HMOUD M., TISLER J., SHIN C., KIM C., WOJCIK A., HEMMER P. R., KRUEGER A., HANKE T., LEITENSTORFER A., BRATSCHITSCH R., JELEZKO F. and WRACHTRUP J., *Nature*, **455** (2008) 648.
- [20] MAZE J. R., STANWIX P. L., HODGES J. S., HONG S., TAYLOR J. M., CAPELLARO P., JIANG L., GURUDEV DUTT M. V., TOGAN E., ZIBROV A. S., YACOBY A., WALSWORTH R. L. and LUKIN M. D., *Nature*, **455** (2008) 644.
- [21] BEVERATOS A., BROURI R., GACOIN T., VILLING A., POIZAT J. P. and GRANGIER P., *Phys. Rev. Lett.*, **89** (2002) 187901.
- [22] GURUDEV DUTT M. V., CHILDRESS L., JIANG L., TOGAN E., MAZE J. R., JELEZKO F., ZIBROV A. S., HEMMER P. R. and LUKIN M. D., *Science*, **316** (2007) 1312.
- [23] RITTWEGER E., HAN K. Y., IRVINE S. E., EGGELING C. and HELL S. W., *Nat. Photonics*, **3** (2009) 144.
- [24] MANSON N. B., HARRISON J. P. and SELLARS M. J., *Phys. Rev. B*, **74** (2006) .
- [25] KURTSIEFER C., MAYER S., ZARDA P. and WEINFURTER H., *Phys. Rev. Lett.*, **85** (2000) 290.
- [26] STAUDT T., LANG M., MEDDA R., ENGELHARDT J. and HELL S. W., *Microsc. Res. Tech.*, **70** (2007) 1.
- [27] HARKE B., KELLER J., ULLAL C. K., WESTPHAL V., SCHOENLE A. and HELL S. W., *Opt. Express*, **16** (2008) 4154.
- [28] HELL S. W., *Phys. Lett. A*, **326** (2004) 140.
- [29] HELL S. W. and SCHÖNLE A., *Nanoscale resolution in far-field fluorescence microscopy*, in *Science of Microscopy*, edited by HAWKES P. W. and SPENCE J. C. H., Vol. **2** (Springer, New York, NY) 2007, pp. 790–834.
- [30] HEISENBERG W., *The Physical Principles of the Quantum Theory* (Chicago University Press, Chicago) 1930.
- [31] BOBROFF N., *Rev. Sci. Instrum.*, **57** (1986) 1152.
- [32] RICHARDSON W. H., *J. Opt. Soc. Am.*, **62** (1972) 55.
- [33] HELL S. W., *Science*, **316** (2007) 1153.
- [34] BETZIG E., PATTERSON G., SOUGRAT R., LINDWASSER O., OLENYCH S., BONIFACINO J., DAVIDSON M., LIPPINCOTT-SCHWARTZ J. and HESS H., *Science*, **313** (2006) 1642.
- [35] RUST M. J., BATES M. and ZHUANG X., *Nat. Methods*, **3** (2006) 793.
- [36] KHAN M. and HEMMER P. R., *Fluctuations and Noise in Photonics and Quantum Optics III*, *Proc. SPIE*, **5842** (2005) 301.
- [37] LAUTERBUR P. C., *Nature*, **242** (1973) 190.